Chapter 1
Thin Film Optical Coatings

Cheng-Chung Lee

1.1 Introduction

Optical thin films are widely used and increasing their importance in nearly all technologies of optics and photonics. They not only improve the optical performance of optical devices, but also are vital parts in optical operations. The films can be composed of dielectric or metallic materials or a combination of the two. The optical thin films discussed in this chapter mainly have a thickness on the order of wavelengths so that optical interference take place, although some are in nano scale and come out from the interaction between electromagnetic waves or photons with electrons in the media and quantum effect has to be considered.

There are many thin films have been applied in optics and photonics, from daily consumer goods to defense and scientific research. The examples are thin films for cell phones, lattices—invisible touch panels, digital cameras, binocular telescopes, CD and DVD, projection TV, TFT LCD display, fax machines, eyeglasses, sunglasses, telecom, LED, Organic LED (OLED), solar cells, smart windows, green buildings, head-up displays, E-cars, security, anti-counterfeiting on documents, currency notes, decorations, telescopes, aircraft, satellites, interferometers, microscopes, fluorescence analysis, plasmonics and biosensors, lasers, nonlinear optics, ultra-short pulse laser mirrors, laser fusion, nanotechnology and metamaterial, etc., covering the spectral ranges from IR to EUV. In terminology those coatings are described as anti-reflection, anti-glare, transparent conduction, high reflection, omni-directional coating, beam splitting neutrally, color separation, UV-IR cut, polarizing separation, non-polarizing filter, long-wave pass, shortwave pass, band pass, band stop or minus or notch or rugate filters, gain flatten, chirped

C.-C. Lee (✉)
Thin Film Technology Center/Department of Optics and Photonics,
National Central University, 300 Chung-Da Road, Chung-Li 32001, Taiwan
e-mail: cclee@dop.ncu.edu.tw

© Springer Science+Business Media Dordrecht 2015

C.-C. Lee (ed.), *The Current Trends of Optics and Photonics*,
Topics in Applied Physics 129, DOI 10.1007/978-94-017-9392-6_1

mirrors, high power laser, interferometry, lighting, display, optical communication, security, energy conversion, colorimetry, thermal management, biophotonics, structural and stratified films, etc.

Although powerful thin film software is very helpful to design an optical thin film assembly to meet the specification through modern numerical synthesis and refinement techniques, the basic theory of optical thin films is still the essential. Some theoretical aspects of optical interference coatings are developed essentially for scientific interest, others are required for progress in optics and photonics. However, the techniques to manufacture thin film interference coatings were developed to satisfy the needs of best performance in optics and photonics. Therefore the challenging requirement in theory and fabrication from optics and photonics are never stopped, particular when nanotechnology, quantum dots and meta-material are concerned.

In this chapter we are not intend to cover all topics, instead, some current technologies about theory, design and manufacture of optical thin films will be described.

1.2 Extra-High Reflection Coating with Negative Extinction Coefficient

A simple metallic film, such as Ag and Al can also act as a high-reflection coating. However, to have low absorption it is necessary to have an all-dielectric multilayer. One may find in nature such as the shell of abalone, scales that any periodic system of stratified layers with alternating high and low refractive indices will give high reflectance, but only the quarter-wave stack has the highest and broadest reflection zone. This is the basic structure for high reflection mirrors and laser cavity mirrors. The basic design of a quarter-wave stack is $S/H(LH)^p/A$, where S is the substrate, A is incident medium, air in general case, and H and L indicate the quarter-wave layers of high and low band filter for DWD. The equivalent refractive index of the quarter wave stack, n_E, can be expressed as in (1.1), where n_S, n_H, and n_L are the substrate index, high and low layers' refractive indices, respectively. It is easy to find that the higher the p, the higher the reflectance, R, from (1.2)

$$n_E = (n_H/n_L)^{2p} n_H^2/n_S. \tag{1.1}$$

$$R = [(1 - n_E)/(1 + n_E)]\,[(1 - n_E)/(1 + n_E)]^*. \tag{1.2}$$

Accordingly, the maximum of R is 0.99999…. but can't equal to 1, not even greater than 1. Recently, an extra-high reflector, eHR, by using multilayers with a negative k, commonly referred to as gain layers was demonstrated that R can be greater than 1 theoretically and experimentally [1].

In theory, the admittance locus of a perfectly dielectric single layer always traces clockwise and forms a circle while an absorbing layer shrinks the circle to

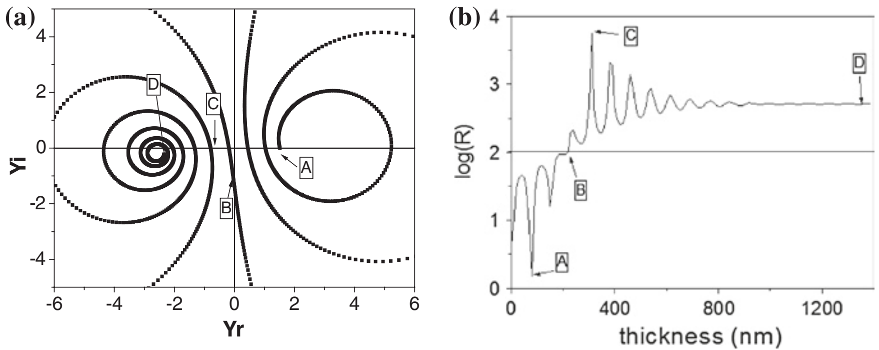

Fig. 1.1 **a** Admittance locus of a gain layers with refractive index n = 2.57 and negative k = −0.2; **b** Corresponding reflectance, *R*, is great than 1 after point B

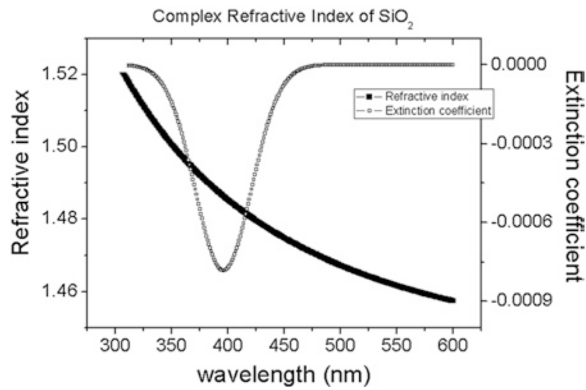

Fig. 1.2 Refractive index and negative extinction coefficient of SiO_2 layer with CdS quantum dots [1]

form a vortex [2]. Instead, the admittance locus of a gain layer expands the circle and spirals anticlockwise when the locus on the left side of the complex plane [3]. Figure 1.1 shows the admittance locus of a gain layers with refractive index n = 2.57, negative extinction coefficient $k = -0.2$ and optical thickness 30H deposed on a substrate with refractive index 1.515. The locus starts from point A, passes to negative side of real part of the admittance axis at point B where the reflectance is greater than 100 % and ends at point D.

The gain layer was fabricated by embedding CdS quantum dots in a dielectric, SiO_2, layer. The effective k value is around −0.0008, as shown in Fig. 1.2 [1]. Let L′ be the gain layer and deposited as the last second layer of a conventional quarter wave stack, $(HL)^8$ L′H. Admittance locus of L′ turns from a conventional clockwise direction into an anticlockwise one. The magnification of the square area of the sub-diagram demonstrates that this transition occurs in the gain layer after a conventional high reflector, HR, as shown in Fig. 1.3. *R* is greater than 1 at wavelength 393 nm as shown in Fig. 1.4 for HRs $(HL)^8$ L′. To push *R* even higher, a H layer is added as the last layer: $(HL)^8$ L′H.

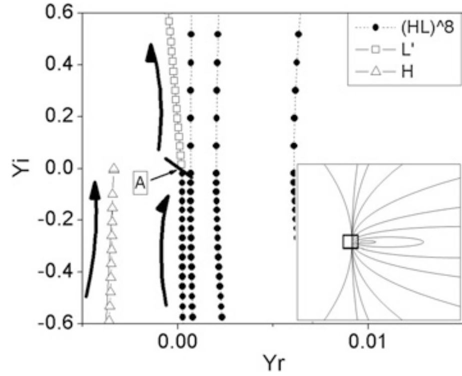

Fig. 1.3 Admittance locus of $(HL)^8$ L′H turns from a conventional clockwise direction into an anticlockwise one. The magnification of the square area of the sub-diagram demonstrates that this transition occurs in the gain layer, L′, after a conventional HR [1]

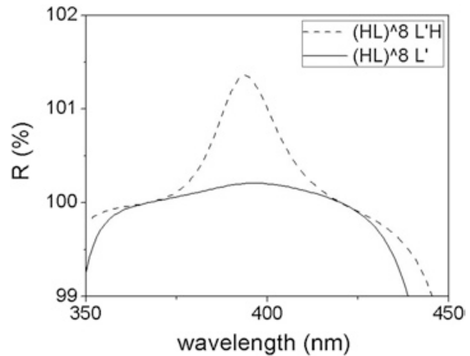

Fig. 1.4 Gain layer L′ improve the reflectance [1]

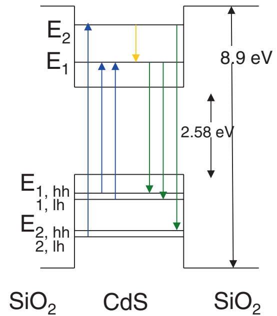

Fig. 1.5 Extra energy at emission wavelength is generated by the down transition owing to the discrete energy levels of quantum dots

A gain medium has a negative extinction coefficient at a specific wavelength. Such unusual behavior does not violate energy conservation. The extra energy at emission wavelength is generated by the down transition owing to the discrete energy levels of quantum dots, explaining why some of the energy associated with shorter wavelengths is transferred to longer wavelengths. Figure 1.5 indicates the energy transfer mechanism. This phenomenon implies that the media provided extra absorption and gain at some specific wavelengths. The application of gain layers is very forward-looking, such as efficiency increase in solar cell [4–7] and LED [8], LD [9], display [10], biology [11] and a loss compensation layer for metamaterials [12–14], etc.

1.3 Narrow Band Pass Filter for Optical Communication with the Half-Peak Bandwidth in Order of Nanometer

One of the techniques to increase the channels so that more optical carrier signals can be multiplexed into a light stream and transmitted on a single optical fiber is utilizing subnano-bandwidth narrow band pass filters, the so called dense wavelength division multiplexing/demultiplexing (DWDM) technology. The design of such filters is based on Fabry-Perot type filter **HR-Sp-HR**, where **HR** is a high reflector which is made of quarter stacks, $(HL)^qH$ or $(HL)^q$ and **Sp** is a multiple half-wave layer called a spacer, *m*2L or *m*2H. The center wavelength λ_0 is determined by the optical thickness of the spacer *nd* and reflection phase shift of HRs ϕ_a and ϕ_b as indicated by (1.3), while half-peak bandwidth $\Delta\lambda_h$ is different for high and low refractive indices spacers and dependent on the order *m* and refractive indices of layers as expressed by (1.4) and (1.5), respectively [2].

$$\frac{1}{\lambda_0} = \frac{1}{2nd} \cdot \left(m + \frac{\phi_a + \phi_b}{2\pi} \right) \tag{1.3}$$

$$\frac{\Delta\lambda_h}{\lambda_0} = \frac{4n_L^{2x-1} n_S}{m\pi n_H^{2x}} \cdot \frac{(n_H - n_L)}{(n_H - n_L + n_L/m)} \text{ for a low - index spacer m2L;} \tag{1.4}$$

$$\frac{\Delta\lambda_h}{\lambda_0} = \frac{4n_L^{2x} n_S}{m\pi n_H^{2x+1}} \cdot \frac{(n_H - n_L)}{(n_H - n_L + n_L/m)} \text{ for a high - index spacer m2H.} \tag{1.5}$$

Taking an *m*th order spacer, we obtain a filter: $S/H(LH)^p m2L(LH)^p HL/A$, where the last layer L is an antireflection coating layer. It is called a single-cavity filter and is approximately triangular in shape. To have a square top and sharp edge, we need multiple cavities, as is the case for example in a three-cavity filter: |HR |Sp|HR|L|HR|Sp|HR|L|HR|Sp|HR|, where L is the coupling layer. Figure 1.6 depicts the spectra of the single (S), two (D) and three-cavity (T) narrow band-pass filters.

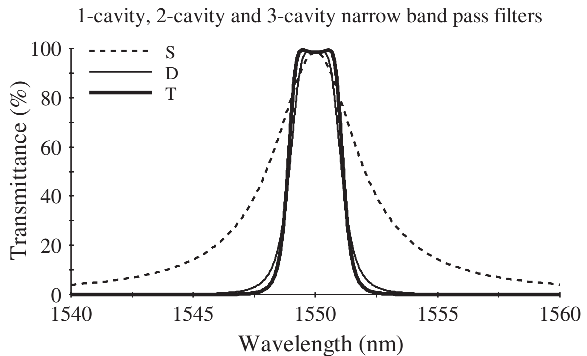

Fig. 1.6 Spectra of single (S), two (D) and three-cavity (T) narrow band-pass filters

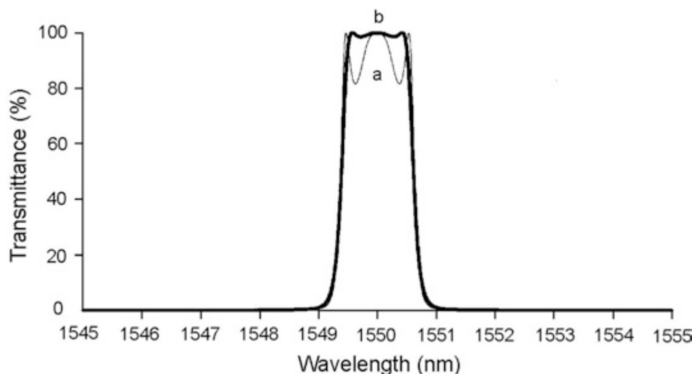

Fig. 1.7 Narrow band pass filter designed by using symmetric layers: **a** S | H L H L H L H L H L H L H L H L[(L H L H L H L H L H L H L H L H) L (H L H L H L H L H L H L H L H L)]^3 L H L H L H L H L H L H L H L H | S, $\lambda_0 = 1{,}500$ nm; **b** S | H L H L H L H L H L H L H L H[(H L H L H L H L H L H L H L H) L (H L H L H L H L H L H L H L H) (4H H L H L H L H L H L H L H) L (H L H L H L H L H L H L H L H 4H) (H L H L H L H L H L H L H L H) L (H L H L H L H L H L H L H L H)]H L H L H L H L H L H L H L H | S [16]

Another approach to design a narrow band pass filter is using the theory of symmetrical combinations of films and the Herpin index, derived by Epstein in 1952 [15]. The equivalent of a symmetric stack with long period such as [(L H L H L H L H L H L H L H L H) L (H L H L H L H L H L H L H L H L)]^3 changes very rapidly such that only a small range of wavelengths can have high transmission. Therefore, such a symmetric assembly potentially can be a narrow band pass filter. Adding matching layers H L H L H L H L H L H L H L H L on both sides of above symmetric assembly, creates a narrow band pass filter for dense wavelength-division multiplexing (DWDM): S/H L H L H L H L H L H L H L H L[(L H L H L H L H L H L H L H L H) L (H L H L H L H L H L H L H L H L)]^3 L H L H L H L H L H L H L H L H/S. The spectrum is shown in Fig. 1.7a. There are two dips in the pass band, yielding features like rabbit ears, which are due to the mismatch of refractive index between the symmetric assembly and its surrounding media. An absentee layer, a multiple of half-wave layer, sometimes called a flattening layer, such as 4H may solve this problem. By adjusting the symmetric assembly and adding 4H in the assembly, the design becomes: S/H L H L H L H L H L H L H L H[(H L H L H L H L H L H L H L H) L (H L H L H L H L H L H L H L H)(4H H L H L H L H L H L H L H) L (H L H L H L H L H L H L H L H 4H) (H L H L H L H L H L H L H L H) L (H L H L H L H L H L H L H L H)]H L H L H L H L H L H L H L H/S. The spectrum is shown in Fig. 1.17b. The rabbit ears are eliminated [16].

The fabrication of such narrow band pass filters for DWDM is very rigorous. Any tiny error may ruin the filter. A narrow band pass filter with layers thickness error 0.0001 will destroy the optical performance as show in Fig. 1.8. The solid line is the designed spectrum and the three dash lines are with standard deviation 0.0001. Figure 1.9 indicates the spectra of a 5-cavity narrow band pass

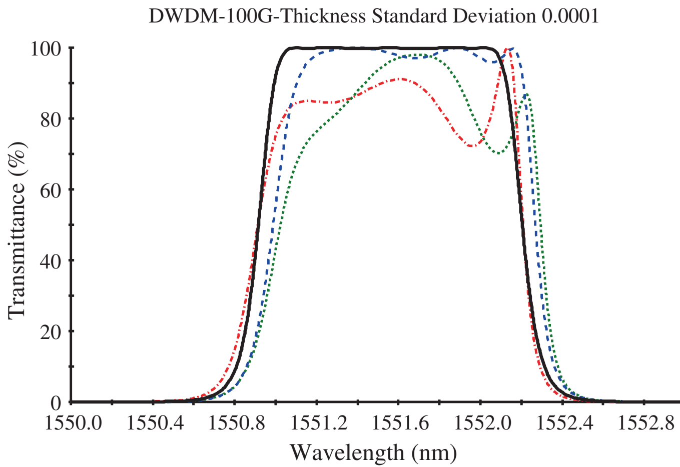

Fig. 1.8 Spectra of a narrow band pass filter with thickness error 0.0001 in each layers

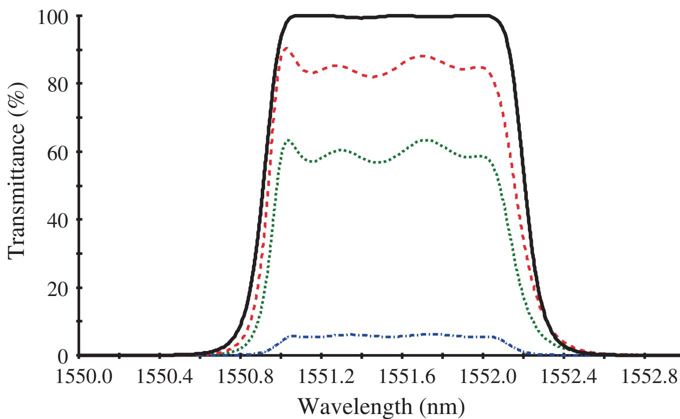

Fig. 1.9 Spectra of a 100 GHz DWD filter with thickness error 0.0005, 0.001 and 0.005 at the last spacer

filter with thickness error 0.0005, 0.001 and 0.005 at the last spacer. All of these explain the thickness error tolerance is very tight. Fortunately, by using error self-compensation effect through turning point optical monitoring, cutting layer with sensitive monitoring wavelength and in situ error compensation, [16–20] we are able to manufacture DWDM filter successfully. Figure 1.10 shows the comparison of designed and fabricated 5-caity narrow band filter for DWDM. The Half-maximum bandwidth $\Delta\lambda_h$ at 3 dB is less than 0.8 nm as required.

Since filters for is extremely sensitive to the optical thickness error in each composite layer. Therefore to have large useful coating area is extreme difficult because of the uniformity problem. For 100 GHz DWDM filters the uniformity

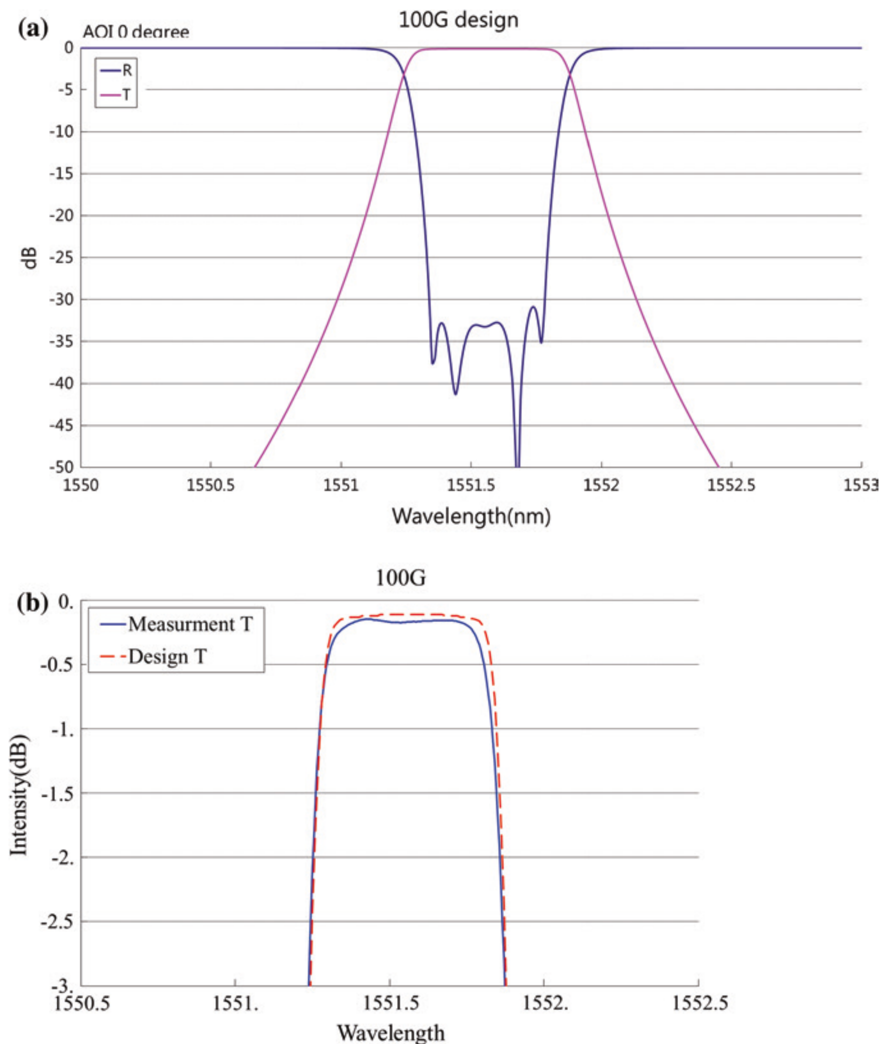

Fig. 1.10 Narrow band pass filter for DWDM, **a** design; **b** comparison of design and fabrication (courtesy of Apogee Optocom Co., Ltd., Taiwan)

must be better than ±0.005 %. The tooling factor, that is ratio of the optical thickness deposited outside the center to the optical thickness deposited at the center, of high and low layers at the different positions are different as indicated by Fig. 1.11 that makes coating a large useful area even difficult.

To enlarge the useful coating area it is necessary to improve the design and the fabrication of DWDM filters. By using an etching technique on the depositing layers with oxygen ion and a new technique, shaping tooling factor, STF, 100 GHz DWDM filters, $S/L(HL)^5\ H10LH(LH)^5\ [L(HL)^6\ H10LH(LH)^6]^3\ L(HL)^5$

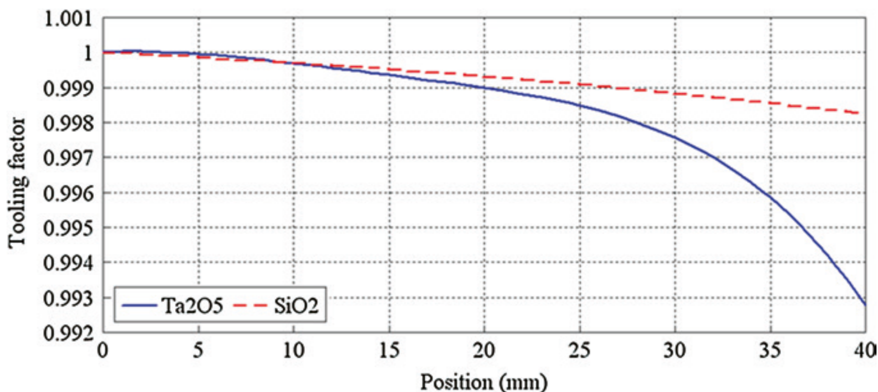

Fig. 1.11 Tooling factors of sources Ta_2O_5 (*solid line*) and SiO_2 (*dash line*)

H10LH(LH)^4 L′H′/Air have been successfully fabricated with the uniformity better than ±0.003 % over an area of 50 mm in diameter and better than ±0.0006 % over a 20 mm in diameter as illustrated by Fig. 1.12 [21].

Since the half-peak bandwidth $\Delta\lambda_h$ is determined by the refractive indices of layers as indicated by (1.4) and (1.5), $\Delta\lambda_h$ is can't be arbitrary. This sometimes will be a problem to make narrow band pass filters for DWDM, coarse WDM, CWDM and 4-skipt-0, etc. By adjusting the coating parameters such as the Ar flow of an ion source in an E-gun in an ion-assisted deposition, IAD, process, to vary the refractive index of the thin film material, one is able to fine tune the bandwidth of a narrow band pass filter to an arbitrary value [22]. The fabrication results are shown in Fig. 1.13 for 4-skipt-0 and CWDM narrow band pass filters.

1.4 Antireflection Coating (AR Coating)

Almost all optics components need anti-reflection coatings not only for increase transmission, but also to eliminate image deterioration due to ghost images and glare. Therefore there are millions of pieces of anti-reflection coatings are processed every day, not including other huge-volume anti-reflection coatings for non-imaging systems, such as solar cells for light absorption and LEDs for light extraction.

In theory a single-layer with a refractive index $n = \sqrt{n}$ can make reflectance $R = 0$. However, there is no robust material where n as small as $\sqrt{n}$. Therefore we need multilayers of alternating TiO_2 or Ta_2O_5 or Nb_2O_5 and SiO_2 to reduce the reflectance. Coated glasses and plastics are much clearer in transmission than an uncoated pair as shown in Fig. 1.14a, b [23]. However, there can still be a residual magenta or green color in reflection as shown in Fig. 1.15. Figure 1.14c shows a green residual color of an antireflection coating on plastics glasses. Coated optical

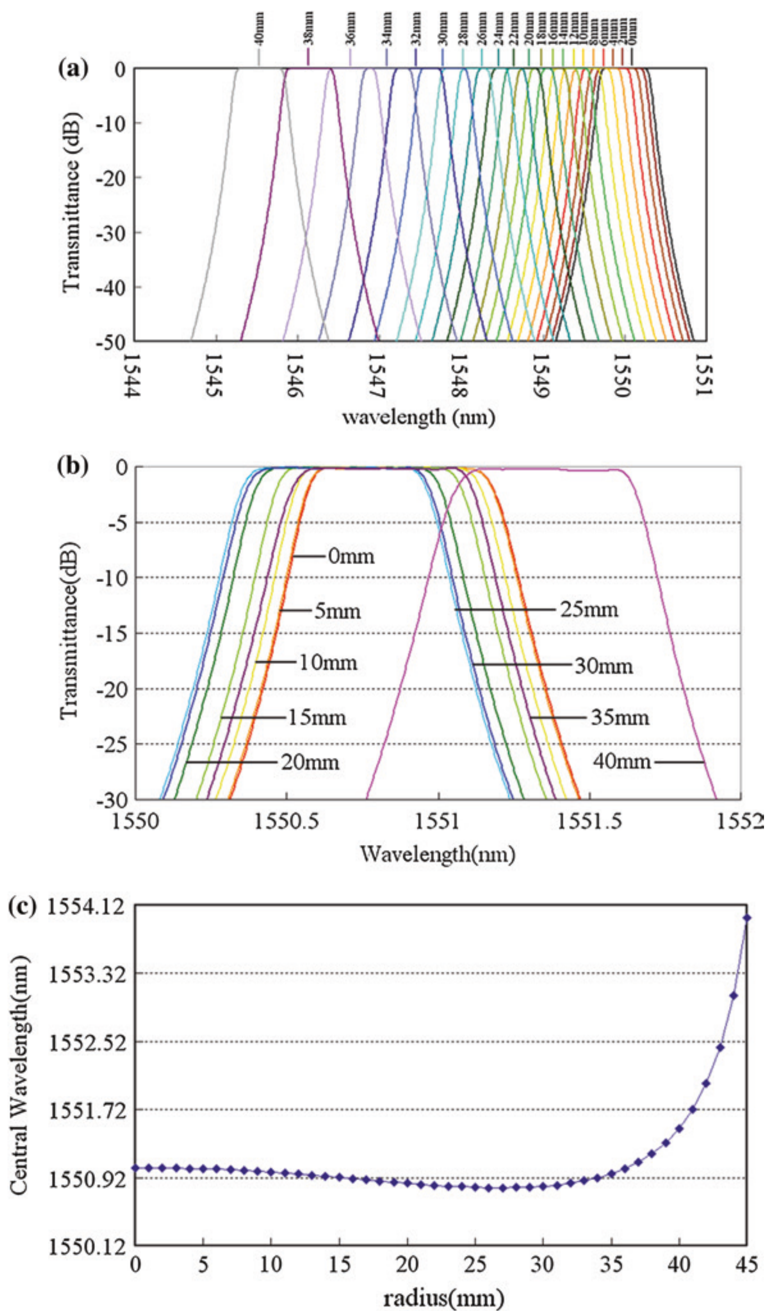

Fig. 1.12 Spectra of the 100 GHz filters measured every 5 mm from the center of the substrate: **a** fabricated by conventional method; **b** by modified method; **c** distribution of the center wavelength on a substrate [21]

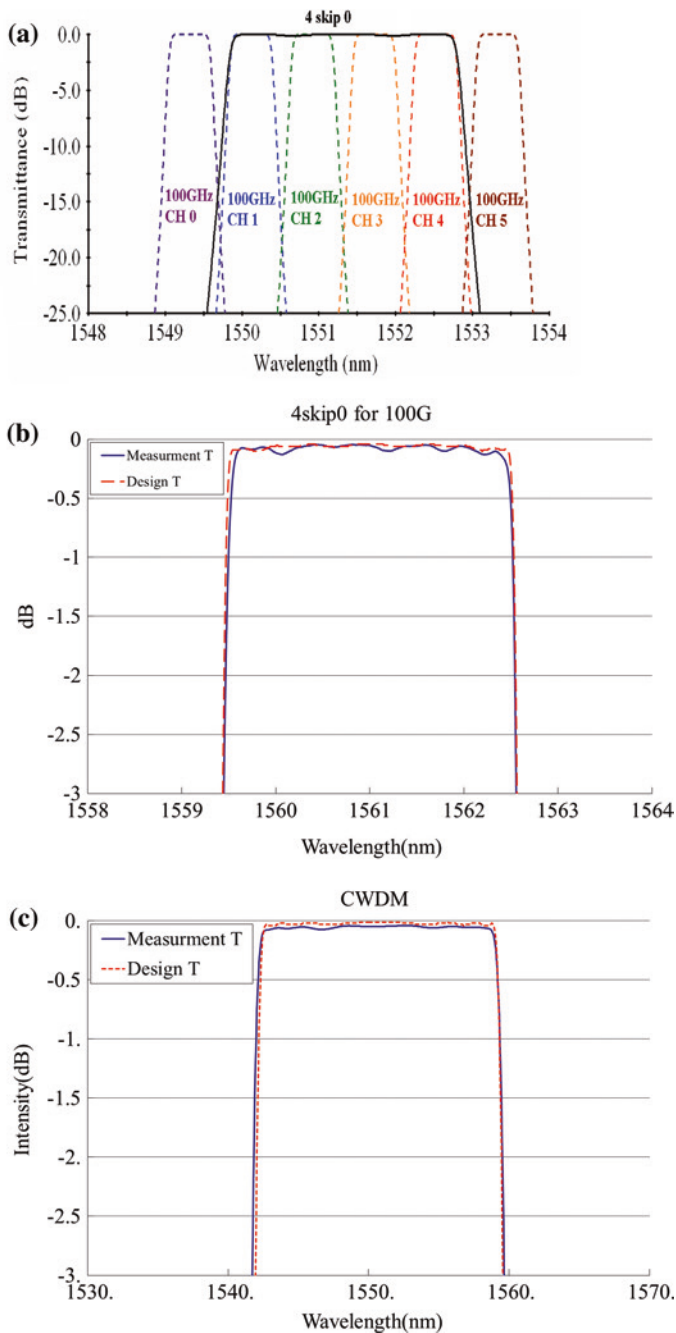

Fig. 1.13 Narrow band pass filter with arbitrary half-peak bandwidth: **a** Sketch of the 4-skip-0 [22]; **b** measured 4-skip-0 filter; **c** measured CWDM filter (courtesy of Apogee Optocom Co., Ltd., Taiwan)

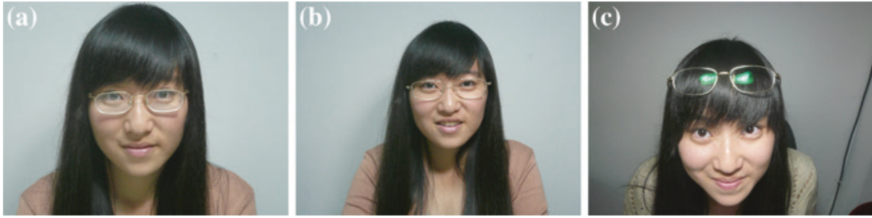

Fig. 1.14 Uncoated glasses **a** and coated glasses **b** and **c**, **c** has residual *green color* in the reflection [23]

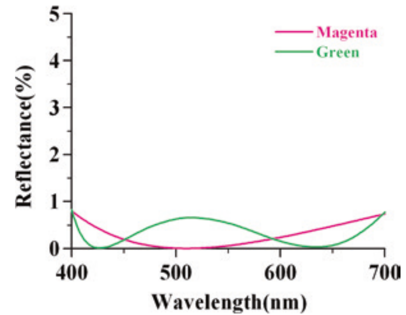

Fig. 1.15 Antireflection coating with residual *magenta* and *green colors*

surfaces in, for example, camera lenses, will frequently display some residual color and this is taken as an indication of the presence of an antireflection coating, no other instruments being necessary for its detection.

To remove the residual color usually implies more layers. Alternatively, an inhomogeneous or gradient index layer has also been proposed. As we understand that a single layer with gradient-refractive-index can represent a broadband wide-angle anti-reflection coating [16, 23, 24]. Such examples occur in nature, the moth eye for example. Researchers have fabricated such films by plasma etching [25, 26], nano-imprint lithography to produce a pyramid array [27], constructing an array of subwavelength-sized features in the form similar to a moth eye [28]. Alternatively, utilize negative refractive index layer may have a broader band and wider angle low reflection, if the negative refractive index layer could be realized [29]. The material with negative refractive index sometimes called as metamaterial which is not easy to fabricate on the conventional substrate with current technology unfortunately. Coatings designed with negative refractive index layer has been will be illustrated in Sect. 1.5. More description about material with negative refractive index will be addressed in Chap. 2.

Nevertheless, in some cases, we may take residual color for decoration. Figure 1.16 shows colored solar cells with different colors without too much loss of efficiency by adjusting the thickness of the layers for antireflection. That gives color appearance of the solar cells. Those solar cells are now in production and

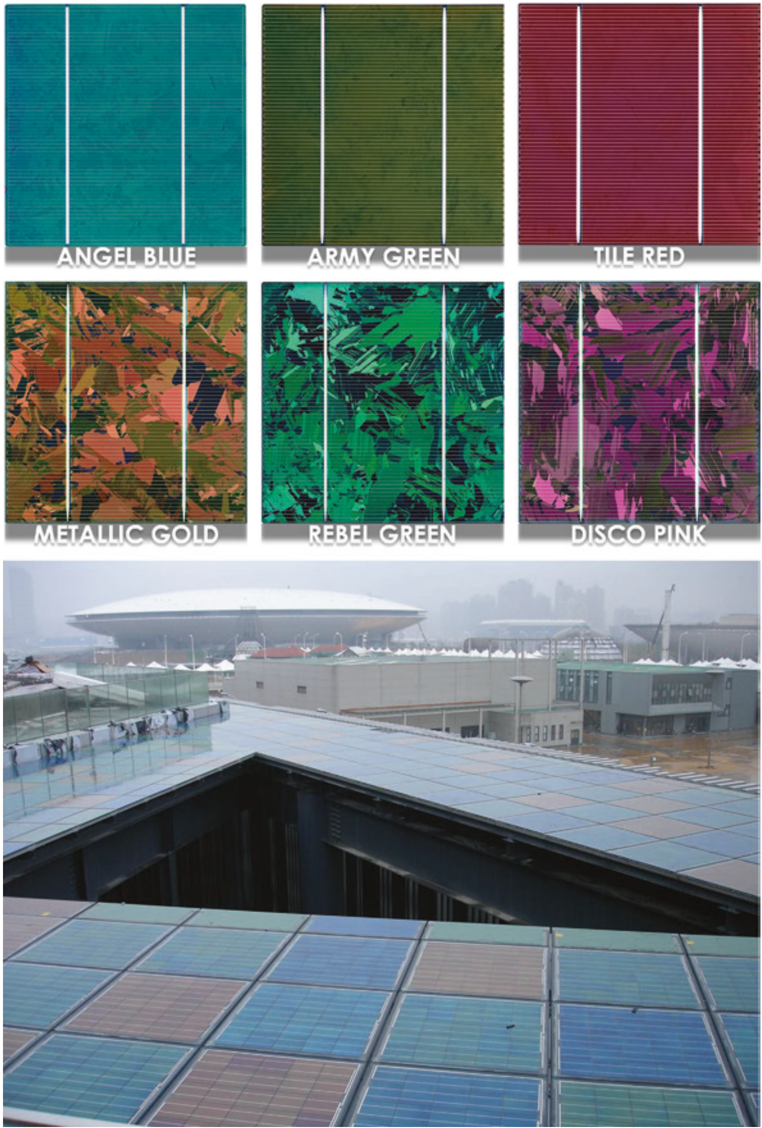

Fig. 1.16 Colored solar cells with different colors installed on the roof of China Pavilion at the Shanghai World Expo 2010 (courtesy of LOF Solar Corp., Taiwan)

have been installed on the roof of the China Pavilion at the Shanghai World Expo 2010, 2012 Yeosu Expo, Italy Bari Airport, Ontario, Utah University, etc.

The anti-reflection and anti-glare coatings to reduce the annoying disturbance from external sources such as bright ambient lights, and to enhance the contrast of the images for the screens of flat panel displays need an absorbing layer combined

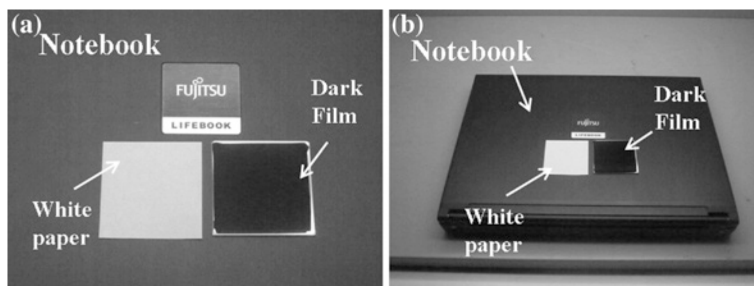

Fig. 1.17 Antireflection coating, *black dark* coating on aluminum made by thin film: **a** normal incidence; **b** oblique incidence [16, 23]

with dielectric layers such as Cr/CrO_x, Fe/FO_x, ITO/SiO_2, $TiNO_x/SiO_2$ [30], and TiN_xW_y/SiO_2 [31] To keep the screen free from contamination, as well as easy to clean with a soft cloth or tissue, a hydrophobic coating has been suggested. The hydrophobic coating should have low surface energy. Usually, the water contact angle should be greater than 110° [32]. Perfluoropolyether polymers modified with organofunctional silanes have been developed to present a hydrophobic surface [33, 34]. However, the durability of such material still needs to be improved. Alternatively, coating a film with nanoroughness has been proposed [35]. Contact angles as high as 152° have been obtained. Instead of hydrophobic coating, applying hydrophilic coating to increase the surface energy of the substrate may split the water droplets and reduce stray light and unwanted reflections. A hydrophilic coating can be realized by short wavelength, such as UV or near UV illumination of photo catalytic material, for example TiO_2 and Nb-doped TiO_2 (TNO) film, so that organic contamination, for example fingerprint, was decomposed through photo-catalysis.

An antireflection for metallic surface may be achieved by utilizing absorbing layers combined with dielectric layers. Figure 1.17 is an example antireflection coating on aluminum plate [16, 23], Al/Nb_2O_5 (36.78 nm)/Nb (12.67 nm)/Nb_2O_5 (28.70 nm)/SiO_2 (61 nm)/Air. Since there is almost no light reflected, it looks very dark and called as “black dark coating” or “dark film”. It is darker than the black note book. It can be even darker if the metal surface is roughed before coating.

1.5 Coatings with Negative Refractive Index Layer

Normally, the phase thickness of optical thin film increases with the thickness of optical thin film. However, the phase thickness of negative refractive index material, NIM decreases as the thickness of the film increases. Therefore NIM might be possible be used for phase compensation in normal thin film design. The result could affect the spectra of the thin films have less sensitivity in wavelength and incident angle.

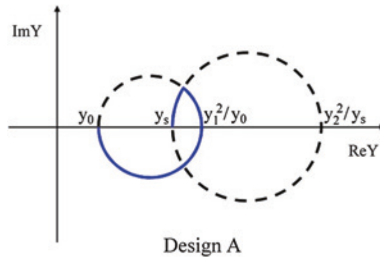

Fig. 1.18 Admittance loci of two-layer V-coat antireflection coating on a glass with refractive index 1.52. The first refractive indices of the first and second layers are 2.23 and 1.45 respectively

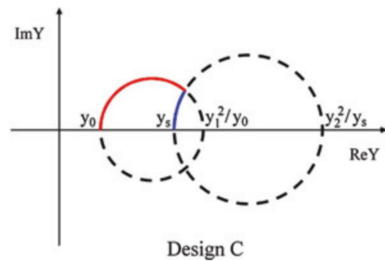

Fig. 1.19 Admittance loci of two-layer V-coat antireflection coating similar to Fig. 1.18, except the refractive index of the second layers is negative, −1.45 (*red color*) [29]

If the antireflection coatings are designed with NIMs, the low reflection range is broader than without NIM and the average reflection is lower. Another application for NIM is to replace the spacer layer using NIM in a narrow band pass filter. Thus the narrow band pass filter can be designed as a wavelength-non-shift filter with incident angle.

Although an antireflection using negative refractive index layer may be not achievable at this moment, it is still interesting to know the advantage of its application. Figure 1.18 shows admittance loci of a two-layer V-coat of antireflection on a glass with refractive index 1.52. The first refractive indices of the first and second layers are 2.23 and 1.45 respectively, let it be design A. All the loci trace in clockwise. Figure 1.19 shows admittance loci of a two-layer V-coat similar as Fig. 1.18 except the refractive index of the second layers is negative, −1.45, let it be design C. The locus of the second layer traces in counterclockwise so that it has phase compensation. It is obvious that the reflectance of design C is much lower over wider spectral range than that of design A as indicated by Fig. 1.20. Figure 1.21 shows that design C is less sensitive in the average reflection from 400 to 700 nm with incident angle than that of design C, particular for S-polarization light.

Usually a filter shows an annoying blue shift in spectrum at tilt angle and s-polarization and p-polarization shift differently. This is particular intolerable for a narrow band pass filter. By utilizing negative refractive index negative layer as

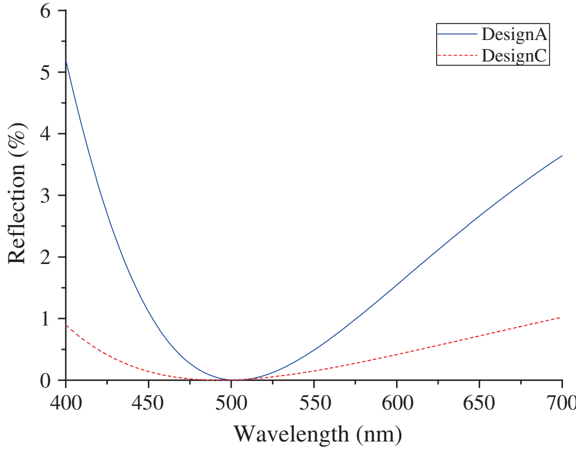

Fig. 1.20 Comparison of reflectance spectra of designs A and C [29]

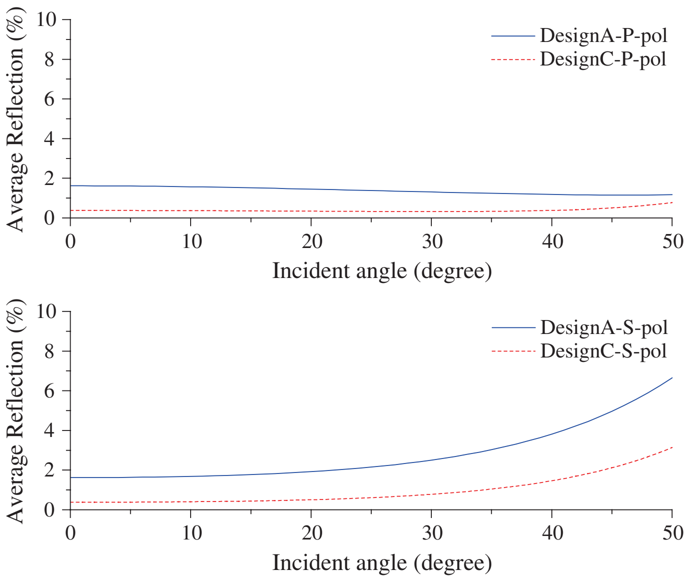

Fig. 1.21 Change of average reflection from 400 to 700 nm with angle for AR designs A and C [29]

one of the spacer can solve this problem. Figure 1.22 is a narrowband pass filter design with NIM layer in the spacer: Sub|$(HL)^7$ H 3NL 6H 3NL H $(LH)^7$|Air. The spacer 3NL 6H 3NL, inserted two three-quarter-wave layers 3NL with negative refractive index −1.47. The shift in peak wavelength is less than 0.1 nm for incident angle 10°, and less than 0.4 nm for s-polarize light and almost no shift for p-polarize light for incident angle up to 18°.

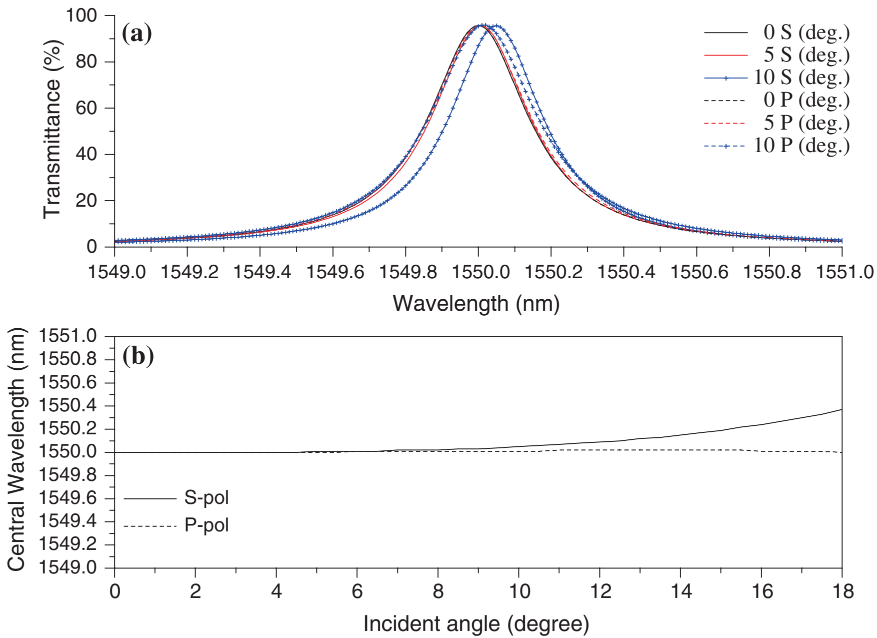

Fig. 1.22 Narrowband pass filter: Sub|(HL)^7 H 3NL 6H 3NL H (LH)^7|Air. H and L are quarter wave layers with refractive indices 2.3 and 1.47 respectively. 3NL is a three-quarter wave layer with negative refractive index −1.47 [29]

1.6 Optical Monitoring

A reliable monitoring for thin film deposition is very important to achieve a theoretical multilayer design. Various monitoring methods, such as time counting, color recognition, quartz monitoring and optical monitoring, have been developed to control thickness during thin-film deposition [17, 18, 36]. Monitoring by time counting is simpler than other monitoring methods, but it needs a very stable deposition rate. Quartz monitoring is also simple but may not be suitable for a coating in plasma environment or a coating with many layers. Besides, in time counting and quartz monitors, the errors in the layer thickness cannot be compensated for and will accumulate with each successively deposited layer. Monitoring by color appearance only works for a simple design. And most of times the operator may loss his/her color cognitive sensitivity after a long looking at the colors. Optical monitoring is based on changes of reflectance (R)/transmittance (T) as the film thickness increases and it has several advantages that to realize a sophisticate design. For example, the turning point method, TPM, is the most commonly used, and has the advantage of error compensation for a coating which composed of quarter-wave layers and multiple of quarter-wave layers [17]. The turning point monitoring is the layer deposition terminated when the signal of R/T reaches its

extreme value. For nonquarterwave stacks, the wavelength of the monitoring system must be changed to an appropriate wavelength for monitoring each individual layer. In this case, the level monitoring method, LM, is more suitable [36]. The so called level monitoring is the deposition of a layer terminated when the signal of reflectance/transmittance reaches its theoretical predicted level. General speaking, the monitoring sensitivity of TPM is low, while in LM, the monitoring wavelength can be selected to make the signals sensitive to changes in thickness near the termination point of the deposition, but the error compensation ability is lower. If *R*/*T* are measured on the coating to be fabricated, we call it is a direct monitoring. It is usually applied on coatings which composed of quarter-wave layers and multiple of quarter-wave layers because of a powerful self-compensation effect. For nonquarterwave stacks, to avoid a rapid error acumination, layer thicknesses are monitored on one or several separate witness chips, and called as indirect monitoring, is applied. Several numerical methods and the optimum trigger point method have been developed to improve the performance, sensitivity and compensation associated with the TPM and the LM methods [18, 37–41].

1.6.1 In Situ Sensitive Optical Monitoring with Error Compensation (ISMEC)

The conventional monitoring methods use runsheet diagrams to control the thickness of the films, based on their transmittance or reflectance, and no phase information can be provided. The fact is that the refractive index n, the extinction coefficient k, and the thickness d are not independently determined in real-time, which make phase extraction difficult. In a growing thin-film stack, the refractive index of the materials may change with time due to variations in the coating parameters or environmental fluctuations in the chamber, meaning we cannot terminate the current layer at the point specified in the original design. Therefore real-time determination of n, k and d is necessary for precision coatings. Ellipsometric and phase extraction methods have been proposed to solve this problem. Ellipsometric monitoring [42, 43] requires algebraic computation to obtain the optical constants that fit the measurements, but require so many parameters that they are difficult to solve analytically. In the case of multilayer coatings, this could lead to the accumulation of errors, which would cause the final optical performance to differ from that of the original design. To avoid this type of error accumulation, in situ sensitivity monitoring with proper error compensation, ISMEC, has been proposed to find the correct refractive index and physical thickness of each deposited layer [20]. An operator can choose the sensitivity monitoring wavelength that offers better error compensation for the reference wavelength. Figure 1.23 shows the experimental results of the monitoring of a narrow band-pass filter with a center wavelength at 800 nm by the ISMEC, TPM and LM methods [20]. The better performance of ISMEC method is clear. The Half-maximum bandwidth $\Delta\lambda_h$ and the position of the maximum

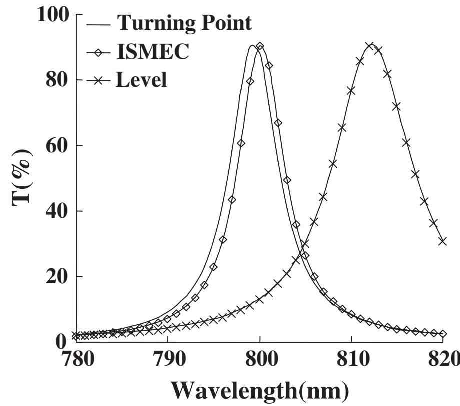

Fig. 1.23 Spectra of narrow band-pass filters monitored by the three methods [20]

transmittance are closer to the designed values than are those obtained using the other two methods. This is because TPM offers error compensation only for previous layers, but lacks sensitivity at termination points, which results in a broadening of the $\Delta\lambda_h$. The level monitoring method has higher sensitivity, but no error compensation, which results in a shift of the output spectrum. ISMEC method on the other hand, combines the advantages of both methods, the sensitivity at termination points and the error compensation for previous layers.

1.6.2 Optical Monitoring and Real Time Admittance Loci Calculation Through Dynamic Interferometer

To get rid of the influence of the variations in the coating parameters caused by environmental fluctuations in the chamber, a polarization Fizeau interferometer-based monitoring system has been developed [44]. This is a vibration-insensitive in situ system, whereby one can instantly obtain the real-time phase and magnitude of the reflection coefficient and/or the transmission coefficient. The layout of a reflection monitoring system with a short coherence light source is shown in Fig. 1.24. The test surface is located on the side of thin film growth, while the other side of the substrate is the reference surface, as shown in Figs. 1.25 and 1.26 for transmission and reflection monitoring system, respectively. The tunable retarder is composed of two wedge x-cut uniaxial birefringent crystals. The crystal-induced phase difference between two orthogonally polarized beams has to match the difference in the optical phase induced by the reference surface and the test surface. The interference will therefore occur only between either the S-polarized reference beam and the P-polarized test beam or the P-polarized reference beam and the S-polarized test beam. Other reflections from the interfaces will be suppressed, because of the short coherence length of the light

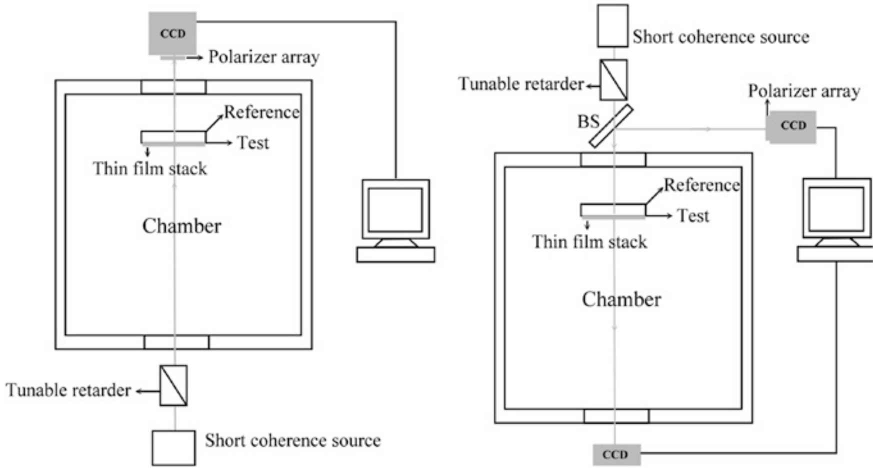

Fig. 1.24 Schematic representation of the transmission and reflection optical monitoring system through dynamic interferometer [44]

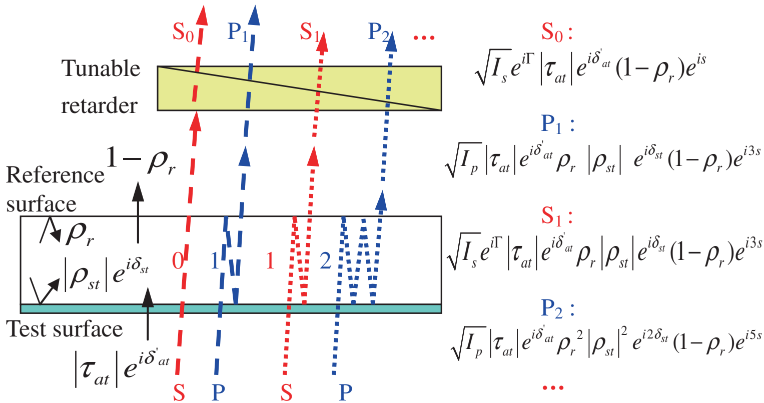

Fig. 1.25 Multiple reflections in the substrate for transmission monitoring system [44]

source [45]. Interference will occur when the transmission axes of the polarizers are oriented 45° and −45° to the fast axis of the birefringent crystal. These two polarizers, as well as the other two (whose transmission axes are oriented 0° and 90° to the fast axis of the birefringent crystal) are combined, and detected by the compact polarizer detector array, as shown in Fig. 1.27. After mathematical analysis using (1.6–1.7), the magnitude of the reflection coefficient and the phase can be acquired from the phase-shifted interferograms of two orthogonal polarization beams on the detector array, where we assumed the transmission coefficient of the film stack (from air to films) is $\tau_{at} = |\tau_{at}| \exp(i\delta_{at})$, the

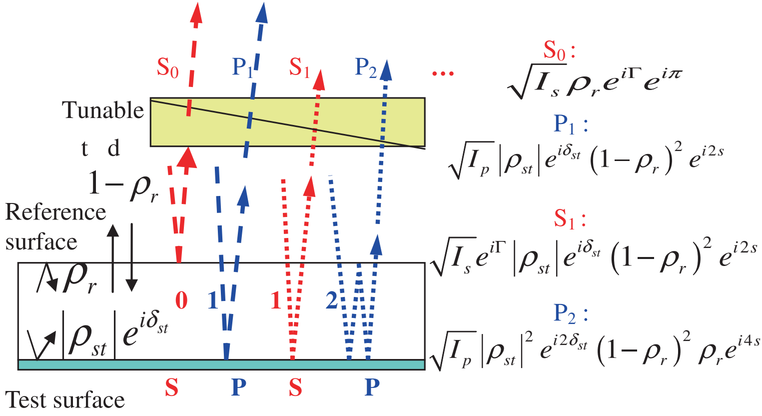

Fig. 1.26 Multiple reflections in the substrate for reflection monitoring system [44]

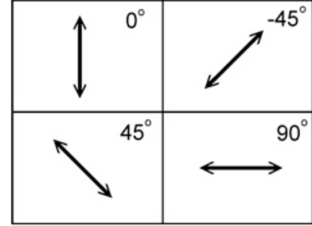

Fig. 1.27 Layout of the polarizer detector array

reflection coefficient of the film stack (from substrate to the deposited film stack) is $\rho_{st} = |\rho_{st}| \exp(i\delta_{st})$, and the reflection magnitude of reference surface (from the substrate to air) is equal to ρ_r. Only the paired beams that are path matched and drawn in the same type of lines will interfere with each other, since the light has short coherence length. The reflection magnitude of the reference surface is assumed equal to ρ_r, and the optical phase difference between two orthogonal polarizations induced by one pass through the substrate and the retarder are s and Γ, respectively. The complete information about the growing film stack thus can be obtained, and the thickness of the whole stack can be monitored accurately.

$$I_{0^\circ} = I_s|\rho_r|^2 + \frac{I_s(1-|\rho_r|)^4|\rho_{st}|^2}{1-|\rho_{st}|^2|\rho_r|^2}, \quad I_{90^\circ} = I_p|\rho_r|^2 + \frac{I_p(1-|\rho_r|)^4|\rho_{st}|^2}{1-|\rho_{st}|^2|\rho_r|^2},$$
$$I_{+45^\circ} = \frac{1}{2}(I_{0^\circ} + I_{90^\circ}) + \sqrt{I_{0^\circ} I_{90^\circ}}|\rho_r||\rho_{st}|\left(1 - \frac{|\rho_r|^2 + (1-|\rho_r|)^2}{\sqrt{I_{0^\circ} I_{90^\circ}}}\right)\cos\theta,$$
$$I_{-45^\circ} = \frac{1}{2}(I_{0^\circ} + I_{90^\circ}) - \sqrt{I_{0^\circ} I_{90^\circ}}|\rho_r||\rho_{st}|\left(1 - \frac{|\rho_r|^2 + (1-|\rho_r|)^2}{\sqrt{I_{0^\circ} I_{90^\circ}}}\right)\cos\theta, \tag{1.6}$$

where I_j is the reflectance of $j = 0°, -45°, +45°$ and $90°$ on the detector array; and $\theta = \phi_{st} + \phi_0$. $\phi_0 = 2s - \Gamma$, is the phase shift caused by the optical path difference between two orthogonal polarizations as they pass through the substrate, s, and the retarder, Γ. ϕ_0 can be acquired before the deposition of the thin film.

$$\phi_{st} = \{\arccos[\frac{\left(I_{+45°} - I_{-45°}\right)}{2\sqrt{I_{0°}I_{90°}}|\rho_r||\rho_{st}|\left(1 - \frac{|\rho_r|^2+(1-|\rho_r|)^2}{\sqrt{I_{0°}I_{90°}}}\right)}]\} - \phi_0. \tag{1.7}$$

Thus by applying an interferometer the optical phase information for a growing film stack can be obtained. Both the magnitude and phase of the reflection coefficient can be found and give us access to the complete information about reflection coefficient, optical admittance, refractive index and actual thickness of the growing film stack at every moment. The optical admittance during the coating process can then be extracted. This system is simple, compact, and will be useful in the fabrication of precision optical coatings.

1.6.3 Optical Monitoring Using Admittance Diagram

Better monitoring performance can be achieved from an admittance diagram than a runsheet diagram, because of the higher sensitivity and larger amount of physical and visual information. It has therefore been proposed that they be used in an optical monitoring method [44, 46–48]. The diagram is obtained by plotting the locus of the effective admittance during the deposition process. Changes in the refractive index during the coating process can be easily observed and immediately compensated for from layer to layer as shown in Fig. 1.28. An error occurred at the first layer, b is the predicted termination point and B is

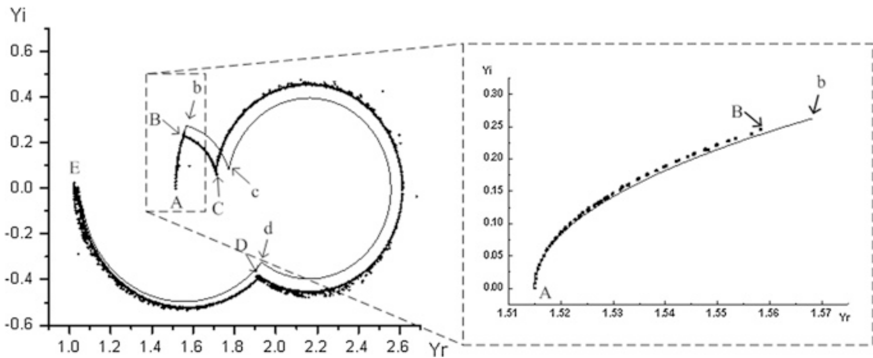

Fig. 1.28 An error occurred at the first layer, *b* is the predicted termination point and *B* is the deposited point. *Thin-solid line* is the simulated loci. In experiment, thickness error was compensated resulting in a new locus, *bold-dot* [48]

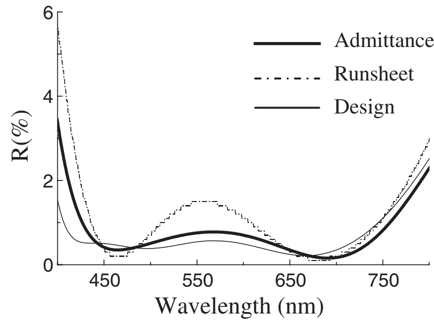

Fig. 1.29 Optical performance of an antireflection coating monitored by the admittance diagram and the conventional runsheet method [48]

the deposited point. The refractive index of the deposited film is higher than the designed film, since the locus is outward expansion. Thin-solid line is the simulated loci. In experiment, thickness error was compensated resulting in a new locus, bold-dot. Figure 1.29 shows plots of the optical performance of an antireflection coating monitored using a real-time admittance diagram and the conventional runsheet method.

1.6.4 Broadband Monitoring Through Equivalent Optical Admittance Loci Observation

The precision of single wavelength monitoring is lower than that of the broadband monitoring, BM, because only one wavelength signal is provided. Not only is it not as comprehensive as broadband monitoring, but the signal errors for the monitoring wavelength dominate the monitoring results. Therefore it is sometimes difficult to obtain the equivalent optical admittance precisely from one single wavelength measurement. Thanks to the highly developed processing technology such as charge-coupled device (CCD) and data extraction and analysis software, the real-time BM is easy to install in a conventional coating machine [49, 50]. In BM, T and/or R values are evaluated simultaneously in different wavelengths. The proper termination time is typically thought to be when the real-time spectrum is the closest to the design spectrum of the termination point. Therefore, a novel method to obtain the refractive index and thickness from the broadband spectrum measurements instead of from a single wavelength measurement and convert this information into the equivalent optical admittance loci of a single wavelength to process the monitor, called as equivalent optical admittance monitoring, EOAM, can be realized [51, 52]. The admittance values can be acquired with higher precision and less noise. This method combines the advantages of both broadband and single wavelength monitors, to let operators terminate the deposition

process at one predicted point, with good error compensation. A 4-layer antireflection coating with physical thicknesses from the first to forth layer are 14 nm (Ta_2O_5), 33 nm (SiO_2), 130 nm (Ta_2O_5), and 85 nm (SiO_2) has been fabricated. In the third and fourth layers, a phase of π was added to the reflection phase, to improve the monitoring sensitivity as shown by Fig. 1.30. The experimental results in Fig. 1.31 clearly show that EOAM performs better than the other methods. A 20 % thickness excess in the 2nd layer has been compensated by the successively deposited layers (Fig. 1.30b). EOAM combines the advantages of the broadband and single-wave monitoring methods without their drawbacks. A phase-adding technique increases the monitoring sensitivity. This should greatly improve the fabrication precision and decrease the defection rate of optical filters, especially for the fabrication of multilayer filters where good error compensation and higher monitoring precision are needed.

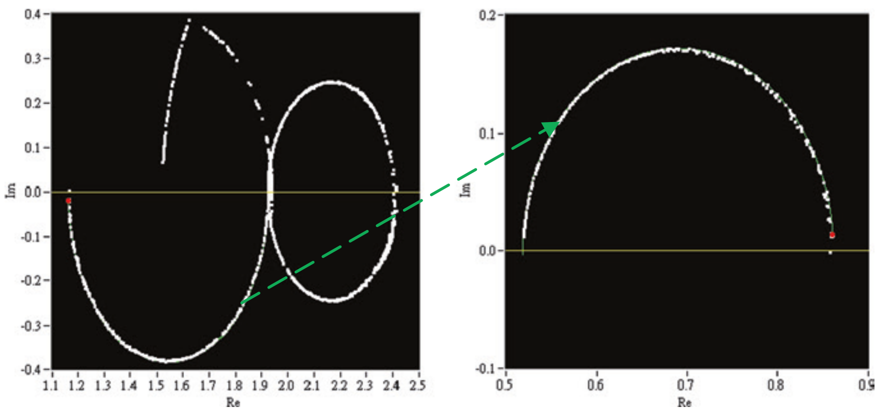

Fig. 1.30 EOAM monitoring loci and the forth layer monitoring locus with phase-shifting technique

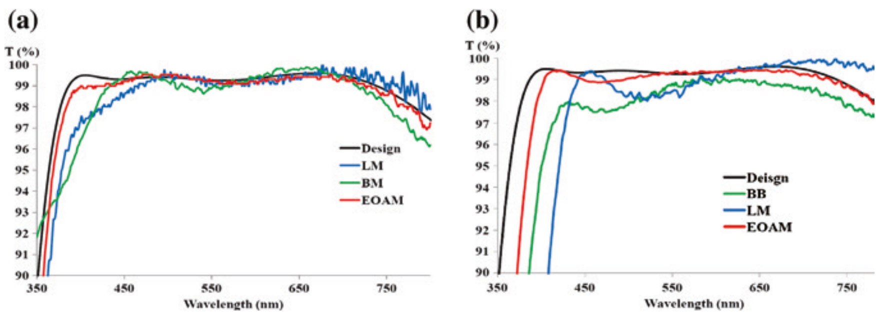

Fig. 1.31 Optical performance of an antireflection coating monitored by various methods: **a** physical thicknesses from the first to forth layer were 14, 33, 130, and 85 nm; **b** 20 % thickness excess in the 2nd layer [51, 52]

1.6.5 Reflection Coefficient Monitoring Through Broadband Spectrum

In this section the reflection coefficient locus will be introduced. Comparing with Turning-Point Monitoring, TPM, Level Monitoring, LM, and Broadband Monitoring, BM, the reflection coefficient monitoring method, RCM, of one single wavelength was acquired through the real time broadband spectrum and it then was used for providing better error compensation and easier termination judgment during the multilayer deposition [53]. BM monitors the real-time broad-band spectrum and terminates the deposition when the real-time spectrum coincides with the design spectrum at the termination point. Therefore, there may be many local minimums of the difference between the real-time spectrum and the design spectrum during the deposition process. In RCM, one wavelength is selected for the reflection coefficient loci monitoring during the coating process. The reflection coefficient, r, is a function of refractive indices n, thicknesses, d, and the monitoring wavelengths. As the thickness grows, the value of r is changed. The monitoring signal changes with respect to the change in thickness is called monitoring sensitivity. If there is noise interference, the sensitivity determines whether the deposition termination point is easy to be correctly judged. Figure 1.32 shows a comparison of the simulation results for the signal change per 5 nm thickness for different optical monitoring methods. The loci are plotted for one layer of Ta_2O_5 film deposited on a glass. The figure shows that the transmittance locus and optical admittance locus monitoring will have low monitoring sensitivity at certain areas. On the other hand, the reflection coefficient has more uniform monitoring sensitivity than the other monitoring methods. For multilayer stacks, the difference in the uniformity of the monitoring sensitivity between the monitoring methods will be enormous in the later deposited layers. The operator can choose a monitoring wavelength that has a larger reflection coefficient change near the deposition termination point for easier judgment of termination. Since only one point can be determined as the termination point, the best choice for termination will be if the deposition is ended when the reflection coefficient at the monitoring wavelength is the closest to its designed value. Similarly, for some coatings which are sensitive to phase variations, the reflection phase provided in this method can be used to precisely terminate the locus at the designed phase.

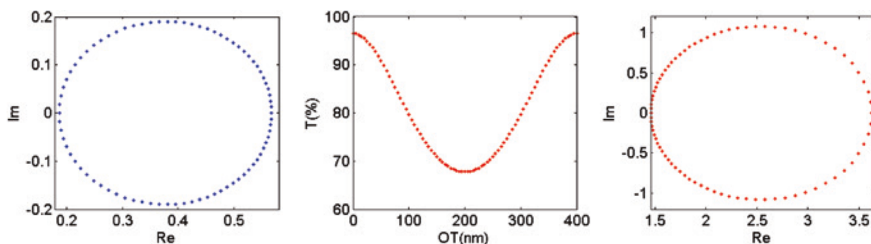

Fig. 1.32 Reflection coefficient, transmittance, and optical admittance loci (from *left* to *right*) [53]

In the monitoring, one wavelength is selected for the reflection coefficient loci monitoring during the coating process. However, for higher precision calculation, the broadband transmittance or reflectance spectrum is used to calculate the real time refractive indices *n*, and thicknesses, *d*, in order to acquire the corresponding reflection coefficient value *r* of the selected wavelength. The deposition of each layer should be terminated when the reflection coefficient value is the closest to the design value. The selected wavelength could be the reference wavelength of the design.

The refractive index, *n*, and thickness, *d*, then can be obtained from the real time broadband spectrum, and derived the reflection coefficient, both of the reflection phase and amplitude, from the obtained refractive index and thickness. The more wavelengths that are used in the calculations, the more accurate will be the *n* and *d* obtained through the numerical algorithm. Then, re-optimization of the design is carried out after the termination of the deposition of each layer. The selected wavelength for the reflection coefficient monitoring may not be one of the wavelengths for T or R measurements. Unlike the general BM using multi-wavelength signals to evaluate the differences in the design, only the reflection coefficient of the monitoring wavelength is used for the monitor. In this way we can avoid ambiguity in finding the minimum of the merit function.

Long-wave pass filters with a total of 14 layers have been fabricated by various monitoring methods with only one monitoring chip through the whole coating process, i.e., direct monitoring, for comparison. An ion-beam sputtering deposition system with an ion beam source 6-cm in diameter was employed to prepare the filters. Ta_2O_5 and SiO_2 were used as the high and low refractive index materials, respectively. The substrate was B270 glass. The intensity of the monitoring light passing through the monitoring chip was measured by a CCD spectrometer. The edge of the long-wave pass filter was designed at 550 nm. Figure 1.33 shows the results of comparisons between different monitoring methods. We can see that the reflection coefficient monitoring, RCM, has the

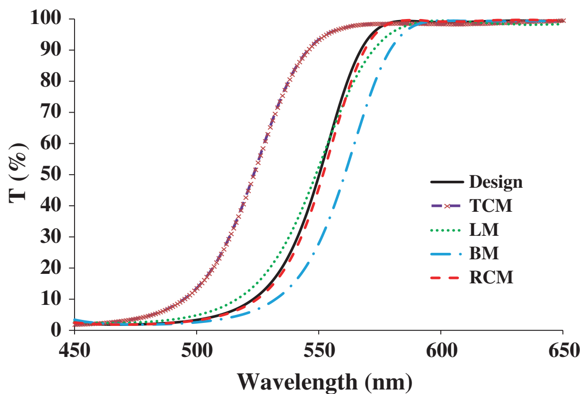

Fig. 1.33 Long-wave pass filters made by various monitoring methods [53]

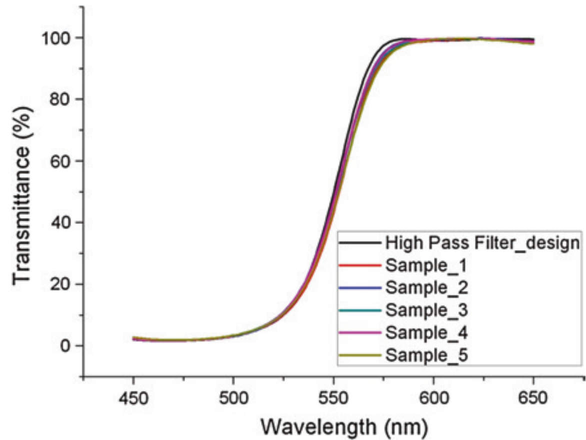

Fig. 1.34 Long-wave pass filters made with direct monitoring for five continuous runs by RCM

best performance. Time Counting Monitoring, TCM, in a stable ion-beam sputtering system has a similar efficiency to quartz monitoring. The accumulated errors introduced a large shift from the design. In Level Monitoring, LM, the position of the spectrum edge was close to the design, but there was obvious distortion in the shape of the spectrum possibly arising from the low precision of thickness control. Broadband monitoring, BM, gives the correct spectrum shape, but the spectrum shift coming from the excess deposition shows the defects. The spectrum of the coating made by RCM was 82 % closer to the design than that made by BM.

When the experiments were done in five continuous runs, the results show that the reflection coefficient monitoring has good error compensation ability, as shown in Fig. 1.34. The shift of the edge from 550 nm (design) was lower than 0.5 %. The reproducibility is also remarkable. In five continuous runs, the shift among each run was below 0.3 %.

In conclusion, the correct choice of monitoring method is extreme important to realize multilayer thin film optical coatings. If thickness error and refractive index change during the deposition are unavoidable, the strategies about optical monitoring for thin film coatings always be the issues. More examples about the strategies of optical monitoring may be found in several articles [54].

1.7 Summary

Optical thin films not only improve the optical performance of optical devices, but also are vital parts in optical operations. The progress of the theory, design and manufacture techniques of optical thin films is never suspended to promote the growth of optics and photonics. Some current technologies about theory, design and manufacture of optical thin films have been described.

The reflectance can be transcended over the limited of quarter wave stacks and photonic crystals, by using gain layer with negative extinction coefficient. Coatings with reflectance more than 100 % have been realized. The gain layer can be made by embedding quantum dots, QDs, in a dielectric film. More information about thin film embedded with QDs can consult with Flory et al. [55–57]. The extra energy at emission wavelength is generated by the down transition owing to the discrete energy levels of quantum dots, so that such unusual behavior does not violate energy conservation. The energy associated with shorter wavelengths is transferred to longer wavelengths. The application of gain layers is very promising, such as efficiency increase in solar cell and LED, LD, display, biology and loss compensation for metamaterials.

The design theory and fabrication techniques of subnano-bandwidth narrow band pass filters are very important and rigorous for dense wavelength division multiplexing/demultiplexing, DWDM, technology. The detail of theory has been introduced and the techniques of coatings has been explained and demonstrated. A useful coating area has been enlarged with the uniformity better than ±0.003 % over an area of 50 mm in diameter and better than ±0.0006 % over a 20 mm in diameter, by using an etching technique on the depositing layers with oxygen ion and a new technique, shaping tooling factor, STF.

Anti-reflection coatings are indispensable for optics elements, since not only transmission can be increased but also image deterioration due to ghost images and glare can be eliminated. The design principle has been explained and some practical antireflection coatings with hydrophobic and hydrophilic characteristics have been investigated. The utilization of the residual color of anti-reflection coatings as a decoration is interesting and has been applied to the solar cells so that the appearance of solar cells is bright and lively but not so dim and gloomy. A black film based on antireflection coating has many applications such for better contrast in display has been designed and fabricated and shown that the black film is darker than a conventional black notebook since almost no light is reflected.

To obtain a theoretical multilayer design needs a reliable monitoring during the thin film deposition. The thickness error of deposited layer and change of refractive during the deposition during the deposition are inevitable and unavoidable. The monitoring technology to achieve the coating as the design one is very crucial. Various advanced monitoring methods, such as in situ sensitive optical monitoring with error compensation, monitoring with real time admittance loci calculation through dynamic interferometer, optical monitoring using admittance diagram, broadband monitoring through equivalent optical admittance loci observation and reflection coefficient monitoring through broadband spectrum have been introduced. Several excellent coatings have been successfully fabricated by utilized the proposed monitoring methods.

Nevertheless, the requests of new technologies about theory, design and manufacture of optical thin films will be tougher and more challenging with the rapid progress in the optics and photonics.

References

1. Y.-J. Chen, C.-C. Lee, S.-H. Chen, F. Flory, Extra-high reflection coating with negative extinction coefficient. Opt. Lett. **38**, 3377–3379 (2013)
2. H.A. Macleod, *Thin-Film optical Filter, 4th ed* (CRC Press, New York, 2010)
3. H.A. Macleod, Gain optical coatings: part 1. Bull. Soc. Vac. Coaters **Issue Fall**, 22–27 (2011)
4. A.J. Nozik, Quantum dot solar cells. Phys. E **14**, 115–120 (2002)
5. Prashant.V. Kamat, Quantum dot solar cells. Semiconductor nanocrystals as light harvesters. J. Phys. Chem. C **112**(48), 18737–18753 (2008)
6. H.-J. Lin, S. Vedraine, J. Le-Rouzo, S.-H. Chen, F. Flory, C.-C. Lee, Optical properties of quantum dots layers: application to photovoltaic solar cells. Sol. Energy Mater. Sol. Cells **117**, 625–656 (2013)
7. J. Wu, Z.M. Wang (eds.), *Quantum Dot Solar Cells* (Springer, New York, 2014)
8. J. Zhao, J.A. Bardecker, A.M. Munro, M.S. Liu, Y. Niu, I.-K. Ding, J. Luo, B. Chen, A.K.-Y. Jen, D.S. Ginger, Efficient CdSe/CdS quantum dot light-emitting diodes using a thermally polymerized hole transport layer. Nano Lett. **6**(3), 463–467 (2006)
9. H. Liu, T. Wang, Q. Jiang, R. Hogg, F. Tutu, F. Pozzi, A. Seeds, Long-wavelength InAs/GaAs quantum-dot laser diode monolithically grown on Ge substrate. Nat. Photonics **5**, 416–419 (2011)
10. T.-H. Kim, K.-S. Cho, E.K. Lee, S.J. Lee, J. Chae, J.W. Kim, D.H. Kim, J.-Y. Kwon, G. Amaratunga, S.Y. Lee, B.L. Choi, Y. Kuk, J.M. Kim, K. Kim, Full-colour quantum dot displays fabricated by transfer printing. Nat. Photonics **5**, 176–182 (2011)
11. S. Jin, Y. Hu, Z. Gu, L. Liu, H.-C. Wu, Application of quantum dots in biological imaging. J. Nanomaterials **2011**(834139) (2011). doi:10.1155/2011/834139
12. A. Fang, T. Koschny, M. Wegener, C.M. Soukoulis, Self-consistent calculation of metamaterials with gain. Phys. Rev. B **79**, 241104(R) (2009)
13. S.M. Xiao, V.P. Drachev, A.V. Kildishev, X.J. Ni, U.K. Chettiar, H.K. Yuan, V.M. Shalaev, Loss-free and active optical negative-index metamaterials. Nature **466**, 735–740 (2010)
14. M. Decker, I. Staude, I.I. Shishkin, K.B. Samusev, P. Parkinson, V.K.A. Sreenivasan, A. Minovich, A.E. Miroshnichenko, A. Zvyagin, C. Jagadish, D.N. Neshev, Y.S. Kivshar, Dual-channel spontaneous emission of quantum dots in magnetic metamaterials. Nat. Commun. **4**(2949) (2013). doi:10.1038/ncomms3949
15. L. Ivan Epstein, The design of optical filter. J. Opt. Soc. Am. **42**, 806–810 (1952)
16. C.-C. Lee, *Thin Film Optics and Coating Technology*, 7th edn. (Yi Hsien, Taipei, 2012)
17. H. Angus Macleod, Turning value monitoring of narrow-band all-dielectric thin-film optical filters. Optica Acta **19**, 1–28 (1972)
18. H.A. Macleod, Monitoring of optical coatings. Appl. Opt. **20**, 82–89 (1981)
19. C.-C. Lee, W. Kai, C.-C. Kuo, S.-H. Chen, Improvement of the optical coating process by cutting layers with sensitive monitor wavelengths. Opt. Express **13**, 4854–4861 (2005)
20. C.-C. Lee, W. Kai, In situ sensitive optical monitoring with error compensation. Opt. Lett. **32**(15), 2118–2120 (2007)
21. C.-C. Lee, S.-H. Chen, C.-C. Kuo, Fabrication of DWDM filters with large useful area. SPIE Optics and Photonics, paper #6286-15, San Diego, USA, 13–17 Aug 2006
22. C.-C. Lee, S.-H. Chen, C.-C. Kuo, C.-Y. Wei, Achievement of an arbitrary bandwidth for a narrow bandpass filter. Opt. Express **15**, 15228–15233 (2007)
23. C.-C. Lee, Optical interference coatings for optics and photonics (Invited). Appl. Opt. **52**, 73–81 (2013)
24. S.R. Kennedy, M.J. Brett, Porous broadband antireflection coating by glancing angle deposition. Appl. Opt. **42**, 4573–4579 (2003)
25. Y.F. Huang, S. Chattopadhyay, Y.J. Jen, C.Y. Peng, T.A. Liu, Y.K. Hsu, C.L. Pan, H.C. Lo, C.H. Hsu, Y.H. Chang, C.S. Lee, K.H. Chen, L.-C. Chen, Improved broadband and quasi-omnidirectional anti-reflection properties with biomimetic silicon nanostructures. Nat. Nanotechnol. **2**, 770–774 (2007)

26. U. Schulz, C. Präfke, C. Gödeker, N. Kaiser, A. Tünnermann, Plasma-etched organic layers for antireflection purposes. Appl. Opt. **50**, C31–C35 (2011)
27. B. Päivänranta, T. Saastamoinen, M. Kuittinen, A wide-angle antireflection surface for the visible spectrum. Nanotechnology **20**, 375301 (2009)
28. J.-Q. Xi, M.F. Schubert, J.K. Kim, E.F. Schubert, M. Chen, S.-Y. Lin, W. Liu, J.A. Smart, Optical thin-film materials with low refractive index for broadband elimination of Fresnel reflection. Nat. Photonics **1**, 176–179 (2007)
29. J.-L. Tsai, Applications of negative refraction index materials for antireflection and narrow band pass filters. MS Thesis, Department of Optics and Photonics, National Central University, Taiwan, 2009
30. H. Ishikawa, B. Lippey, in *Two layer broad band AR coating*. Proceedings of 10th International Conference on Vacuum Web Coating (Bakish Materials Corporation, 1996), pp. 221–233
31. G. McHale, N.J. Shirtcliffe, M.I. Newton, Contact-angle hysteresis on super-hydrophobic surfaces. Langmuir **20**, 10146–10149 (2004)
32. L. Mascia, T. Tang, Polyperfluoroether-silica hybrids. Polymer **39**, 3045–3057 (1998)
33. K.C. Camargo, A.F. Michels, F.S. Rodembusch, M.F. Kuhn, F. Horowitz, Visibly transparent and near infrared, wideangle, anti-reflection coatings with simultaneous selfcleaning on glass. Opt. Mater. Express **2**, 969–977 (2012)
34. M. Flemming, A. Duparre, Design and characterization of nanostructured ultrahydrophobic coatings. Appl. Opt. **45**, 1397–1401 (2006)
35. K. Zhang, F. Zhu, C.H.A. Huan, A.T.S. Wee, Indium tin oxide films prepared by radio frequency magnetron sputtering method at a low processing temperature. Thin Solid Films **376**, 255–263 (2000)
36. B. Vidal, A. Fornier, E. Pelletier, Wideband optical monitoring of nonquarter wave multilayer filter. Appl. Opt. **18**, 3851–3856 (1979)
37. F. Zhao, Monitoring of periodic multilayer by the level method. Appl. Opt. **24**, 3339–3343 (1985)
38. C.J. van der Laan, Optical monitoring of nonquarterwave stacks. Appl. Opt. **25**, 753–760 (1986)
39. B. Bobbs, J.E. Rudisill, Optical monitoring of nonquarterwave film thickness using a turning point method. Appl. Opt. **26**, 3136–3139 (1987)
40. C. Zang, Y. Wang, W. Lu, A single-wavelength monitoring method for optical thin-film coatings. Opt. Eng. **43**, 1439–1443 (2004)
41. A.V. Tikhonravov, M.K. Trubetskov, Eliminating of cumulative effect of thickness errors in monochromatic monitoring of optical coating production: theory. Appl. Opt. **46**, 2084–2090 (2007)
42. J. Lee, R.W. Collins, Real-time characterization of film growth on transparent substrates by rotating-compensator multichannel ellipsometry. Appl. Opt. **37**, 4230–4238 (1998)
43. S. Dligatch, R. Netterfield, B. Martin, Application of in-situ ellipsometry to the fabrication of multi-layered coatings with sub-nanometre accuracy. Thin Solid Films **455–456**, 376–379 (2004)
44. C.C. Lee, K. Wu, S.H. Chen, S.J. Ma, Optical monitoring and real time admittance loci calculation through polarization interferometer. Opt. Exp. **15**, 17536–17541 (2007)
45. B. Kimbrough, J. Millerd, J. Wyant, J. Hayes, Low coherence vibration insensitive Fizeau interferometer. Proc. SPIE **6292**, 62920F (2006)
46. Y.R. Chen, Monitoring of film growth by admittance diagram. Master Thesis, National Central University, Taiwan, 2004
47. B.J. Chun, C.K. Hwangbo, J.S. Kim, Optical monitoring of nonquarterwave layers of dielectric multilayer filters using optical admittance. Opt. Express **14**, 2473–2480 (2006)
48. C.-C. Lee, Y.J. Chen, Multilayer coatings monitoring using admittance diagram. Opt. Express **16**(9), 6119–6124 (2008)
49. S. Wilbrandt, N. Kaiser, O. Stenzel, In-situ broadband monitoring of heterogeneous optical coatings. Thin Solid Films **502**, 153–157 (2005)

50. B. Badoil, F. Lemarchand, M. Cathelinaud, M. Lequime, Interest of broadband optical monitoring for thin-film filter manufacturing. Appl. Opt. **46**, 4294–4303 (2007)
51. W. Kai, C.-C. Lee, T.-L. Ni, Advanced broadband monitoring for thin film deposition through equivalent optical admittance loci observation. Opt. Express **20**, 3883–3889 (2012)
52. C.C. Lee, K. Wu, T.L. Ni, *Optical Admittance Loci Monitoring for Thin Film Deposition* (Lambert Academic, Saarbrücken, 2012) (ISBN 978-3-659-00198-7)
53. C.-C. Lee, W. Kai, M.-Y. Ho, Reflection coefficient monitoring for optical interference coating depositions. Opt. Lett. **38**, 1325–1327 (2013)
54. A.V. Tikhonravov, T.V. Amotchkina, in *Optical Thin Film and Coatings*, ed. by A. Piegariand, F. Flory. Optical monitoring strategies for optical coating manufacturing, Chap. 3 (Woodhead, Cambridge, 2013). (ISBN 978-0-85709-594-7) (2013)
55. F. Flory, Y.J. Chen, C.C. Lee, L. Escoubas, J.J. Simon, P. Torchio, J. Le Rouzo, Optical properties of dielectric thin films including quantum dots. Appl. Opt. **50**, C129–C134 (2011)
56. F. Flory, L. Escoubas, G. Berginc, optical properties of nanostructured materials a review. Nanophotonics **5**(1), 052502 (2011). doi:10.1117/1.3609266
57. A. Sytchkova, in *Optical Thin Film and Coatings*, ed. by A. Piegariand, F. Flory. Complex materials with plasmonic effects for optical thin film application, Chap. 5 and F. Flory, Y.J. Chen, H.L. Lin, Optical thin films containing quantum dots, Chap. 12 (Woodhead, Cambridge, 2013). (ISBN 978-0-85709-594-7)